

# RSC Advances



This is an *Accepted Manuscript*, which has been through the Royal Society of Chemistry peer review process and has been accepted for publication.

*Accepted Manuscripts* are published online shortly after acceptance, before technical editing, formatting and proof reading. Using this free service, authors can make their results available to the community, in citable form, before we publish the edited article. This *Accepted Manuscript* will be replaced by the edited, formatted and paginated article as soon as this is available.

You can find more information about *Accepted Manuscripts* in the [Information for Authors](#).

Please note that technical editing may introduce minor changes to the text and/or graphics, which may alter content. The journal's standard [Terms & Conditions](#) and the [Ethical guidelines](#) still apply. In no event shall the Royal Society of Chemistry be held responsible for any errors or omissions in this *Accepted Manuscript* or any consequences arising from the use of any information it contains.

# **Biocompatible multiblock aliphatic polyesters containing ether-linkages: influence of molecular architecture on solid-state properties and hydrolysis rate**

*M. Gigli<sup>1</sup>, M. Govoni<sup>2</sup>, N. Lotti<sup>1\*</sup>, E. Giordano<sup>2,3</sup>, M. Gazzano<sup>4</sup>, A. Munari<sup>1</sup>*

<sup>1</sup>Civil, Chemical, Environmental and Materials Engineering Department, University of Bologna, Bologna, Italy.

<sup>2</sup>BioEngLab, Health Science and Technology-Interdepartmental Center for Industrial Research (HST-CIRI), University of Bologna, Ozzano Emilia (BO), Italy

<sup>3</sup>Laboratory of Cellular and Molecular Engineering “Silvio Cavalcanti”, Department of Electrical, Electronic, and Information Engineering “G. Marconi” (DEI), University of Bologna, Cesena (FC), Italy;

<sup>4</sup>Institute for the Organic Synthesis and Photoreactivity, CNR, Bologna, Italy.

\*Correspondence to. Tel: +39-051-2090354; Fax: +39-051-2090322.

*e-mail address: nadia.lotti@unibo.it*

**ABSTRACT**

In this study, we propose a new class of multiblock copolyesters containing butylene 1,4-cyclohexanedicarboxylate (BCE) and diethylene glycol 1,4-cyclohexanedicarboxylate (DGCE) sequences. The two parent homopolymers were prepared by the usual two-stage melt polycondensation. On the other hand, the multiblock copolyesters, characterized by the same chemical composition but different block lengths, were synthesized by reactive blending. Physicochemical characterization (DSC, WAXS, tensile tests, WCA, hydrolysis experiments) demonstrated that the block length controls the polymer crystallinity, the thermal and mechanical properties, the wettability and the degradation rate. The copolymers displayed different stiffness, mainly depending on the crystallinity degree and macromolecular chain flexibility, a tunable range of degradation rates, and different surface hydrophilicity. Biocompatibility assays showed the absence of potentially cytotoxic products released into the culture medium by the investigated samples, and demonstrated that our substrates support a physical environment where cells can adhere and proliferate, confirming their potential for biomedical applications.

**Keywords:** multiblock copolymers; ether linkages; solid-state properties; hydrolytic degradation; biocompatibility.

## 1. INTRODUCTION

Tissue engineering is a multidisciplinary research field - involving medicine, biology, materials science and engineering – aiming at the fabrication of living tissue substitutes for human therapy. Engineering a pseudotissue *in vitro* for subsequent engraftment *in vivo* is a presently exploited strategy where a scaffold provides a structured environment working as an artificial extracellular matrix to support regeneration holding onboard specific cell populations of interest.<sup>1-3</sup>

The scaffold is expected to serve as a biomimetic template for cell adhesion, proliferation and differentiation and, intuitively, its ability to integrate with surrounding tissue-specific mechanical properties represents a critical property. Biomaterials used for scaffold fabrication include biological molecules (e.g., alginate, collagen, fibrin, and hyaluronan) and biomimetic synthetic polymers (e.g., polylactic and polyglycolic acids and their copolymers, polycaprolactone) to sustain the differentiation and functional organization of the seeded cells.<sup>4-6</sup>

Bioengineered tissues such as skin, cartilage and bone<sup>7-9</sup> are already a clinical option available to patients. However, regenerating soft tissues, e.g. muscle, is a present clinical research challenge, because the elastic stretchability is the major mechanical prerequisite of these tissues and, although many efforts have been invested into the development of elastomeric biomaterials that mimic that of native tissue, the replication of their complex behaviour is still unsolved. To this purpose, the study and development of new elastomeric materials have notably increased in the last decade and biodegradable polyurethanes, trimethylene carbonate-based polymers, sebacate and adipate-based polymers and citric acid-based elastomers have been proposed for these applications.<sup>10-15</sup>

Among the techniques employed to realize new polymers with promising properties for tissue engineering applications, reactive blending undoubtedly represent a simple and versatile solvent-free method to synthesize copolymers displaying tuneable properties, which depend on the type, relative amount, and distribution of the comonomeric units.<sup>16-18</sup> Our group recently focused its research activity on the introduction of etheroatoms along the polymeric chain of aliphatic

polyesters, mainly poly(butylene succinate) (PBS); this strategy allowed us to modulate the ability to crystallize of the resulting polymers, and, above all, to enhance their flexibility and surface hydrophilicity.<sup>19-24</sup>

However, the presence of significant amounts of a comonomeric unit in the backbone of parent homopolymer, usually causes a dramatic decrease in the melting point, hindering their use in real applications. To overcome this problem, the use of homopolymers with a high melting point would therefore be preferable. Unfortunately, most of the aliphatic polyesters do not present this characteristic, as the  $T_m$  of PBS, 114°C, is one of the highest among polycondensates.

In this respect, poly(butylene 1,4-*trans*-cyclohexanedicarboxylate) (PBCE) can offer an interesting solution. This aliphatic polyester is in fact characterized by the presence of an aliphatic ring in the monomeric unit which confers very interesting properties: a very high melting point ( $T_m = 166$  °C), good thermal stability, even higher than the aromatic counterpart, poly(butylene terephthalate (PBT)),<sup>25</sup> interesting mechanical properties and biodegradability.<sup>26</sup>

In this study, we propose a new class of multiblock copolyesters containing butylene 1,4-cyclohexanedicarboxylate (BCE) and diethylene glycol 1,4-cyclohexanedicarboxylate (DGCE) sequences, together with the two parent homopolymers. These last were synthesized by the usual two-stage melt polycondensation, while various copolymers of different block length were prepared by reactive blending. The main aim of this work is to evaluate how the molecular architecture influences the thermo-mechanical properties, the wetting behavior, and the hydrolytic degradation profile of the copolyesters under investigation. In view of biomedical applications, the biocompatibility of these new materials has been as well tested by using the H9c2 cell line, derived from embryonic rat heart, as a muscle cell model.<sup>27-28</sup>

## 2. EXPERIMENTAL

### 2.1. Materials

*Trans*-cyclohexane-1,4-dicarboxylic acid (CEDA) was purchased from Zentek (partner of TCI, Milan, Italy), while all the other reagents used were obtained by Sigma Aldrich (Milan, Italy). CEDA, 1,4-butanediol (BD) and diethylene glycol (DG) were reagent grade products and were used without any further purification. Titanium tetrabutoxide ( $\text{Ti}(\text{OBu})_4$ ) (Sigma-Aldrich), was distilled before use.

### 2.2 Synthesis of homopolymers

Poly(butylene 1,4-cyclohexanedicarboxylate) (PBCE) and poly(diethylene glycol 1,4-cyclohexanedicarboxylate) (PDGCE) were synthesized in bulk starting from *trans*-cyclohexane-1,4-dicarboxylic acid and the appropriate glycol in a molar ratio of 1:1,2.  $\text{Ti}(\text{OBu})_4$  was used as catalyst, with the addition of about 150 ppm of Ti/g of theoretical polymer. The syntheses were carried out in a 250 ml stirred glass reactor, with a thermostated silicon oil bath; temperature and torque were continuously recorded during the polymerization.

The polymers were prepared according to the usual two-stage polymerization procedure. In the first stage, under pure nitrogen flow, the temperature was raised over 180 °C and kept there until more than 90% of the theoretical amount of water was distilled off (about 2 hours). In the second stage the pressure was reduced to about 0.1 mbar in order to facilitate the removal of the excess glycol and the temperature was raised to 250 °C; the polymerizations were carried out until a constant torque value was measured.

### 2.3 Synthesis of poly(butylene/diethylene glycol 1,4-cyclohexanedicarboxylate) copolyesters

Poly(butylene/diethylene glycol 1,4-cyclohexanedicarboxylate) copolyesters were obtained by melt mixing non-purified PBCE and PDGCE (1:1 molar ratio of the repeat units) in a 200 mL glass reactor at 240 °C under nitrogen atmosphere to prevent oxidative degradation. During the process, samples were taken from the reactor at different reaction times (30, 50, 120, 220, and 300 min) and

cooled in air. Copolymer formation was catalyzed by the residual titanium tetrabutoxide introduced in the polymerization of PBCE and PDGCE. The copolyesters obtained and analyzed in this work are indicated as P(BCE<sub>x</sub>DGCE<sub>y</sub>), where x and y are the average value of sequence length of BCE and DGCE units, respectively.

#### 2.4. Film preparation

Films (about 0.2 mm thick) of PBCE homopolymer and of P(BCE<sub>x</sub>DGCE<sub>y</sub>) copolymers (PDGCE was impossible to process into films, being a rubber at T<sub>amb</sub>) were obtained by compression molding the polymers between Teflon plates (0.3 mm thick), with an appropriate spacer, at a temperature  $T = T_m + 40$  °C for 2 min under a pressure of 2 ton/m<sup>2</sup> (Carver C12, laboratory press). Prior to characterization, films were kept under ambient temperature for at least 2 weeks in order to attain equilibrium crystallinity.

#### 2.5. Molecular characterization

##### 2.5.1. Nuclear magnetic resonance (NMR)

The polymer structure and actual copolymer composition were determined by means of <sup>1</sup>H-NMR spectroscopy (polymer concentration of 0.5 wt%, a relaxation delay of 1 s, an acquisition time of 1 s, 64 repetitions), whereas the distribution of the comonomeric sequences was evaluated by means of <sup>13</sup>C-NMR spectroscopy (5 wt% solutions and a full decoupling mode with a NOE effect, a relaxation delay of 2 s, an acquisition time of 1 s, 512 repetitions). Chloroform-d was used as solvent and the spectra were recorded at RT by using a Varian INOVA 400 MHz instrument.

##### 2.5.2. Gel permeation chromatography (GPC)

Molecular weight data were obtained by GPC at 30 °C using a 1100 Hewlett Packard system equipped with a PL gel 5m MiniMIX-C column and a refractive index detector. Chloroform was used as eluent with a 0.3 ml min<sup>-1</sup> flow and sample concentrations of about 2 mg ml<sup>-1</sup> were applied. Polystyrene standards in the range of molecular weight 2000–100000 were used.

## 2.6. Thermal characterization

### 2.6.1. Thermogravimetric analysis (TGA)

TGA was carried out both in air and under nitrogen atmosphere using a Perkin Elmer TGA7 apparatus (gas flow: 30 ml/min) at 10 °C/min heating rate up to 900 °C.

### 2.6.2. Differential scanning calorimetry (DSC)

Calorimetric measurements were carried out by means of a Perkin Elmer DSC7 instrument. To measure the glass transition and the melting temperatures, the external block temperature control was set at -120 °C and weighed samples of c.a. 10 mg encapsulated in aluminium pans were heated up to 40 °C above fusion temperature at a rate of 20 °C/min (1<sup>st</sup> scan), held for 3 min, and then rapidly quenched (about 100 °C/min) to -80 °C. Finally, they were reheated from -80 °C to a temperature well above the melting point of the sample at a heating rate of 20 °C/min (2<sup>nd</sup> scan).

In order to determine the crystallization rate under non-isothermal conditions, the samples were cooled from the melt at 5 °C/min. The temperature corresponding to the maximum of the exothermic peak in the DSC cooling-curve ( $T_{cc}$ ) has been correlated to the crystallization rate.

### 2.7. Wide-angle X-ray measurements (WAXD)

X-ray diffraction (XRD) patterns of polymeric films were carried out by using a PANalytical X'PertPro diffractometer equipped with a fast solid state X'Celerator detector and a copper target ( $\lambda = 1.5418 \text{ \AA}$ ). Data were acquired in the 5-60° 2 $\theta$  interval, by collecting 100 sec at each 0.10° step. The indices of crystallinity ( $X_c$ ) were evaluated from the XRD profiles by the ratio between the crystalline diffraction area ( $A_c$ ) and the total area of the diffraction profile ( $A_t$ ). The crystalline diffraction area has been obtained from the total area of the diffraction profile by subtracting the amorphous halo (modelled as bell shaped peak baseline). The non-coherent scattering was taken into consideration.

### 2.8. Mechanical characterization

Stress-strain measurements were performed on rectangular films (5 mm wide and 0.2 mm thick) using an Instron 4465 tensile testing machine equipped with a 100N load cell. The gauge length was equal 20 mm and the cross-head speed was set to 5.0 mm/min. Tensile elastic modulus was determined from the first linear segment of the stress-strain curve. At least six replicates were run for each sample and the results were provided as the average  $\pm$  standard deviation.

### 2.9. Surface wettability

Static contact angle measurements were performed on polymer films by using a KSV CAM101 instrument at ambient conditions by recording the side profiles of deionized water drops for image analysis. Up to ten drops were observed on different area for each film and contact angles were reported as the average value  $\pm$  standard deviation.

### 2.10. Hydrolytic degradation experiments

Prior to degradation experiments each specimen was dried over  $P_2O_5$  under vacuum at RT to constant weight and initial mass was measured. Films were individually immersed in phosphate buffered solution (0.1 M, pH = 7.4, periodically changed to keep the pH constant) and incubated in a SW22 Julabo shaking water bath at 37 °C and 50 rpm. At different time intervals, triplicate specimens for each sample were recovered, repeatedly washed with deionized water and dried over  $P_2O_5$  under vacuum to constant weight. Mass loss was gravimetrically determined.

### 2.11. Biocompatibility studies

#### 2.11.1 Indirect cytotoxicity

Indirect cytotoxicity evaluations of PBCE homo-polymer and  $P(BCE_xDGCE_y)$  copolymers were performed in accordance with the ISO10993-5 international standard for biological evaluation of medical devices, as previous described.<sup>29</sup> Briefly, PrestoBlue<sup>®</sup> (Life Technologies, Monza, Italy). fluorescence (Ex/Em = 540/590 nm) was read in three separate experiments (n = 3), two replicates

each. Mean  $\pm$  standard error of the mean were calculated, and the one-way ANOVA was used to evaluate statistical differences between samples.

### 2.11.2 Cell adhesion and proliferation

Evaluation of both cell adhesion and cell proliferation was performed in accordance with ISO10993-5 as previous described.<sup>30</sup>

The amount of viable cells was quantified at day 1, 7, and 14 using the PrestoBlue<sup>®</sup> fluorescence assay. Control signal was acquired from H9c2 cells cultured in standard (PS) polystyrene wells. Two separate experiments, two replicates each, were performed. Fluorescence values were expressed as mean  $\pm$  standard error of the mean. Comparison between groups was performed using the one-way ANOVA with Tukey's as post-test and differences were considered significant for  $p < 0.05$ .

### 2.12 RNA Isolation and Gene Expression Profile

Total RNA was extracted from H9c2 seeded on various polymer surfaces using TRIzol<sup>®</sup> reagent (Life Technologies, Monza, Italy) and chloroform (Sigma-Aldrich, Milan, Italy) and reverse transcribed as previous described.<sup>31</sup> Real time RT-PCR analysis was performed using the SYBR Premix Ex Taq II (TaKaRa, Tokyo, Japan) with the primers listed in Table 1 and 50 ng cDNA for each reaction. Data were normalized to GAPDH expression (endogenous control). Fold-changes in gene expression were determined by the  $2^{-\Delta\Delta C_q}$  method and are presented relative to levels in H9c2 cultured in PS standard wells. Duplicate experiments were performed.

**Table 1.** Primer sequences.

Primer Names	Primer Sequence 5'-3'	Product size (bp)
<b>GAPDH <i>fw</i></b>	CCT CCT CAT TGA CCT CAA CTA C	312
<b>GAPDH <i>rv</i></b>	CAT GGT GGT GAA GAC GCC AG	
<b>MHC <i>fw</i></b>	TGG CAC CGT GGA CTA CAA TA	100
<b>MHC <i>rv</i></b>	TAC AGG TGC ATC AGC TCC AG	

### 3. RESULTS AND DISCUSSION

#### 3.1 Polymer molecular characterization

PBCE and  $P(\text{BCE}_x\text{DGCE}_y)$  copolymers are opaque and light-yellow colored solid powders, whereas PDGCE is a sticky rubber at RT.

Chemical structures are reported in Figure 1. PBCE and PDGCE homopolymers display a similar chemical structure, both containing two ester groups along a chain containing an aliphatic ring. The only difference between the two polyesters involves the presence of an ether-oxygen atom in the glycol sub-unit of PDGCE.

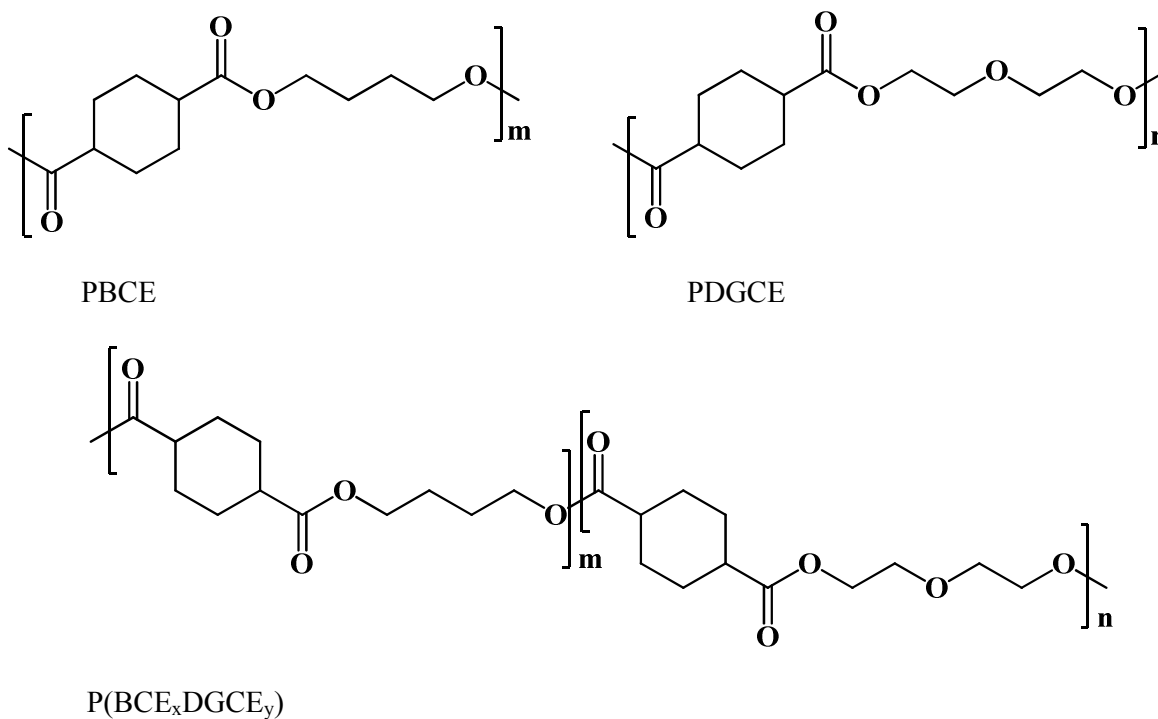


**Figure 1.** Chemical structure of PBCE, PDGCE and  $P(\text{BCE}_x\text{DGCE}_y)$  multiblock copolymers.

To synthesize the multiblock copolymers under study, several preliminary runs carried out at different reaction temperatures were performed (220, 230, 235, 240 and 250°C), in order to optimize mixing conditions. The best temperature turned out to be 240°C.

Data concerning polymer molecular characterization are reported in Table 2. Both PBCE and PDGCE homopolymers, as well as the synthesized copolyesters, were characterized by relatively high molecular weight (Figure 2).

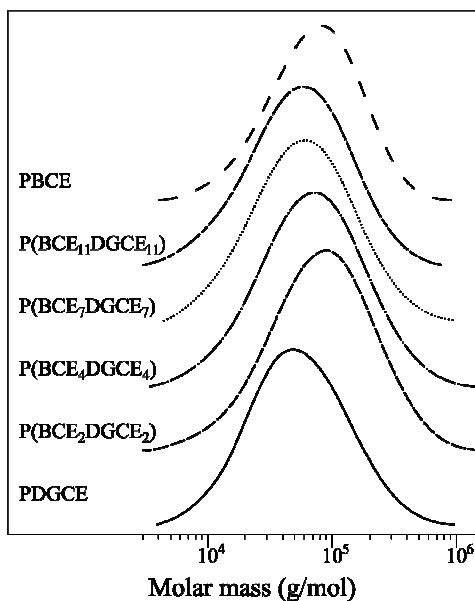


**Figure 2.** Stack plot of GPC traces of PBCE, PDGCE and their copolymers. RI signal is reported as a function of molar mass (g/mol).

This result indicates that during polymer synthesis no appreciable thermal degradation occurred. As already reported,<sup>17</sup> in the case of copolymers an increase of molecular weight with the increasing of reaction time was observed (Table 2), due to the prevalence of transesterification reactions over chain scission ones for longer mixing times.

<sup>1</sup>H-NMR spectra of the two homopolymers (Figure 3) and of the copolymers were found to be consistent with the expected structure. As an example, the <sup>1</sup>H-NMR spectrum for P(BCE<sub>7</sub>DGCE<sub>7</sub>) is shown in Figure 4, together with the chemical shift assignments. The copolymer composition was calculated from the relative areas of the <sup>1</sup>H-NMR resonance peaks of the **e** aliphatic protons of the butanediol subunit, located at 4.10 ppm, and of the **g** protons of the methylene groups of the diethylene diol subunit at 4.25 ppm.

Table 2 shows that in all cases the actual molar composition did not depend on reaction time and was close to the feed one (equimolar content of BCE and DGCE units).

**Table 2.** Molecular characterization data for PBCE, PDGCE and P(BCE<sub>x</sub>DGCE<sub>y</sub>) copolymers.

Polymer	M <sub>n</sub> <sup>1)</sup>	D <sup>2)</sup>	BCE (mol %) <sup>3)</sup>	L <sub>BCE</sub> <sup>4)</sup>	L <sub>DGCE</sub> <sup>4)</sup>	b <sup>5)</sup>
PBCE	48400	2.0	100	/	/	/
P(BCE <sub>11</sub> DGCE <sub>11</sub> )	34600	2.3	50.6	11	11	0.18
P(BCE <sub>7</sub> DGCE <sub>7</sub> )	38600	2.3	49.9	7	7	0.28
P(BCE <sub>4</sub> DGCE <sub>4</sub> )	42500	2.5	49.9	4	4	0.52
P(BCE <sub>2</sub> DGCE <sub>2</sub> )	49400	2.5	52.5	2	2	1.02
PDGCE	36000	2.2	0	/	/	/

<sup>1)</sup>number average molecular weight (GPC);

<sup>2)</sup>polydispersity index (GPC);

<sup>3)</sup>real composition (<sup>1</sup>H-NMR);

<sup>4)</sup>block length sequences (<sup>13</sup>C-NMR);

<sup>5)</sup>degree of randomness (<sup>13</sup>C-NMR).

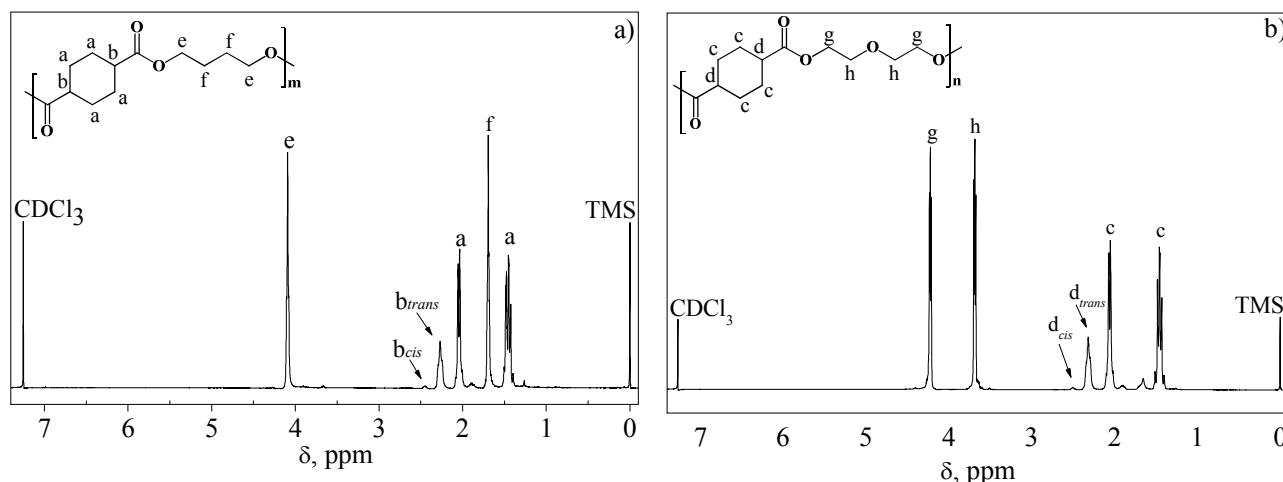


**Figure 3.** <sup>1</sup>H-NMR spectra of: a) PBCE, b) PDGCE with resonance assignments.

<sup>1</sup>H-NMR spectra were also used to calculate the *trans* percentage in the polymers under study; as a matter of fact, 1,4-cyclohexylene ring present in CEDA could isomerize during polymer synthesis, moving toward the thermodynamically stable *cis/trans* ratio of 34-66%. The ratio of the areas of the signals centred at 2.28 ppm (*trans* isomer) and 2.44 ppm (*cis* isomer) was considered for this

calculation. The data obtained indicated that isomerization from the *trans* form to the *cis* one occurred only to small extent during polymerization (*cis* content in all cases less than 2%).

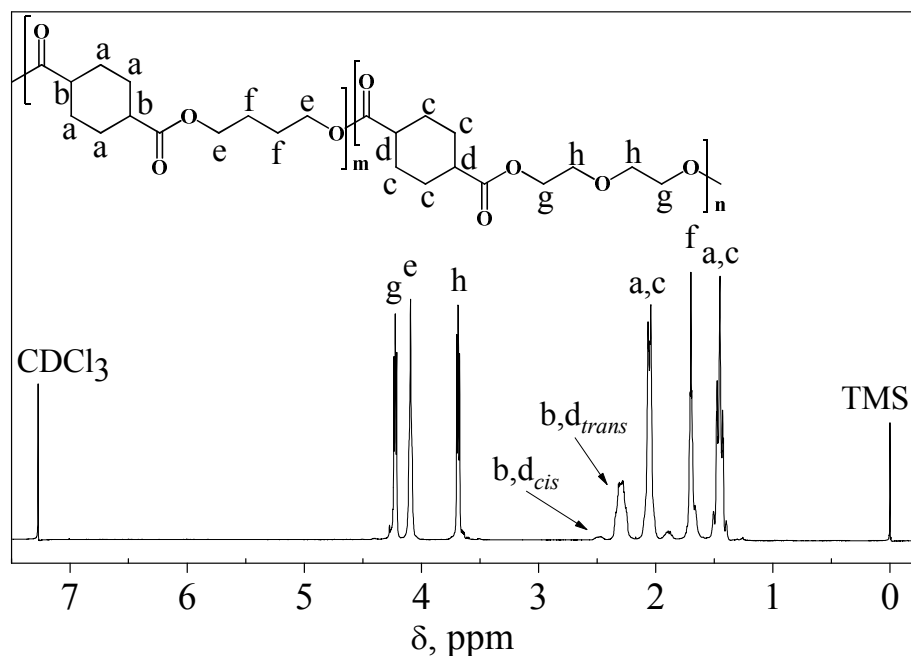


**Figure 4.** <sup>1</sup>H-NMR spectra of P(BCE<sub>7</sub>DGCE<sub>7</sub>) with resonance assignments.

In order to study the molecular structural changes occurring in the course of the reactive blending, <sup>13</sup>C-NMR was employed (Figure 5). In particular, for the copolymers new peaks appeared in the region between  $\delta = 27.8$  and  $\delta = 28.1$ , due to the mixed BCE and DGCE sequences, whose intensity increased with increasing mixing time. Copolymer microstructure was deduced by the degree of randomness (*b*), calculated from <sup>13</sup>C-NMR data. It is well known that *b* is equal to 1 for random copolymers, 2 for alternate copolymers, close to zero for a mixture of two homopolymers, and  $0 < b < 1$  for block copolymers. The degree of randomness was calculated according to the procedure described in the following:

$$b = P_{B-DG} + P_{DG-B} \quad (1)$$

where  $P_{B-DG}$  and  $P_{DG-B}$  are the probability of finding a *B* unit next to a unit *DG* and the probability of finding a *DG* unit next to a unit *B*, respectively.

The two probabilities can be expressed as:

$$P_{B-DG} = \frac{(I_{B-DG} + I_{DG-B})/2}{(I_{B-DG} + I_{DG-B})/2 + I_{B-B}} \quad (2)$$

$$P_{DG-CE} = \frac{(I_{DG-B} + I_{B-DG})/2}{(I_{DG-B} + I_{B-DG})/2 + I_{DG-DG}} \quad (3)$$

where  $I_{B-DG}$ ,  $I_{DG-B}$ ,  $I_{B-B}$  and  $I_{DG-DG}$  represent the integrated intensities of the resonance signals of  $B$ - $DG$ ,  $DG$ - $B$ ,  $B$ - $B$ , and  $DG$ - $DG$  sequences, respectively.

Additionally, the average length of the PBCE and PDGCE sequences in the copolymer are defined as:

$$L_{BCE} = 1/P_{B-DG} \quad (4)$$

$$L_{DGCE} = 1/P_{DG-B} \quad (5)$$

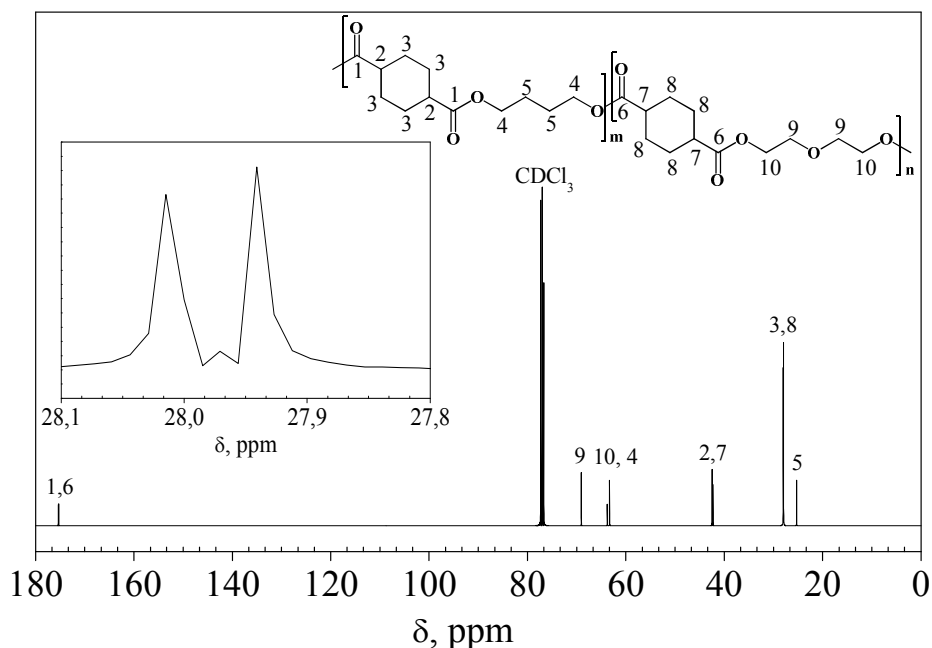


**Figure 5.**  $^{13}\text{C}$ -NMR spectra of P(BCE<sub>7</sub>DGCE<sub>7</sub>) with resonance assignments and an enlargement of the region between 27.8 and 28.1 ppm.

The average BCE and DGCE sequence length and the degree of randomness of P(BCE<sub>x</sub>DGCE<sub>y</sub>) copolyesters are reported in Table 2. Increasing the mixing time decreased the average block length

and increased the degree of randomness, confirming the proceeding of transesterification reactions. Therefore, the evolution from a block architecture (P(BCE<sub>11</sub>DGCE<sub>11</sub>)) to a random one (P(BCE<sub>2</sub>DGCE<sub>2</sub>)) was observed with increasing mixing time.

In order to investigate the relative hydrophilicity of PBCE, and P(BCE<sub>x</sub>DGCE<sub>y</sub>) films, water contact angle (WCA) measurements were performed. Given the identical chemical composition of the investigated copolymers (i.e. BCE : DGCE = 50 : 50 mol%), material hydrophilicity should be expected to be the same in all cases. Table 3 reports the contact angle values for each polymer. The data showed that PBCE was the most hydrophobic material and that the introduction of an ether-oxygen atom per repeating unit resulted in increasing material hydrophilicity. In the case of copolyesters, similar WCA values were found. Therefore, copolymerization of PBCE with PDGCE permits to obtain a new class of block copolymers which are more hydrophilic than PBCE, due to the presence along the polymer chain of polar oxygen atoms.

### 3.2. Polymer thermal properties and crystallization ability

The polyesters were afterwards examined by thermogravimetric analysis and differential scanning calorimetry. The investigation on the thermal stability was carried out both in air and under nitrogen atmosphere. From the thermogravimetric curves of some samples under nitrogen atmosphere shown in Figure 6, the temperature of 5% of weight loss ( $T_{5\%}$ ) and the temperature corresponding to the maximum weight loss rate ( $T_{max}$ ) were determined and collected in Table 3. In all cases the weight loss takes place practically in one-step and is 100%. From the comparison between the TGA curves of PBCE and PDGCE, one can see that the ether-oxygen-containing polyester is more thermally stable than PBCE (see  $T_{max}$ ).

Taking into account that among the various degradation mechanisms proposed to explain the thermal degradation reactions occurring in polyesters, the random cleavage of covalent bonds of the polymeric chains can be invoked, the higher stability of PDGCE with respect of PBCE can be explained on the basis of the higher energy of the C-O bond with respect to C-C one. As far as

P(BCE<sub>x</sub>DGCE<sub>y</sub>) copolymers are concerned, their thermal stability was found good, similar and intermediate between those of parent homopolymers ( $T_{max}$  ranging from 431 to 434 °C in Table 3).

**Table 3.** Thermal, diffractometric data and water contact angles for PBCE, PDGCE and P(BCE<sub>x</sub>DGCE<sub>y</sub>) copolymers.

Polymer	$T_{5\%}$ (°C)	$T_{max}$ (°C)	1 <sup>st</sup> scan		2 <sup>nd</sup> scan						$T_{cc}$ (°C)	$X_c$	WCA°
			$T_m$ (°C)	$\Delta H_m$ (J/g)	$T_g$ (°C)	$\Delta C_p$ (J/°C·g)	$T_c$ (°C)	$\Delta H_c$ (J/g)	$T_m$ (°C)	$\Delta H_m$ (J/g)			
PBCE	388	422	167	30	12	0.059	/	/	166	28	144	42 ± 3	110 ± 2
P(BCE <sub>11</sub> DGCE <sub>11</sub> )	385	434	150	17	-5	0.232	/	/	149	16	128	26 ± 3	89 ± 1
P(BCE <sub>7</sub> DGCE <sub>7</sub> )	385	434	140	17	-5	0.237	/	/	140	16	117	25 ± 3	88 ± 2
P(BCE <sub>4</sub> DGCE <sub>4</sub> )	389	433	120	15	-3	0.200	/	/	120	15	94	21 ± 3	89 ± 1
P(BCE <sub>2</sub> DGCE <sub>2</sub> )	386	431	95	13	-2	0.301	50	12	95	12	59	n.d.	87 ± 2
PDGCE	385	451	/	/	-7	0.370	/	/	/	/	/	/	/

As regards calorimetric results, being the samples characterized by high  $M_n$ s, an influence of molecular weight on the glass transition and melting of the polymers synthesized can be excluded.

It is well established that the melting behaviour of a polymer is affected by its previous thermal history and therefore, in order to provide the same heat treatment to all the samples investigated, as mentioned above, prior to thermal analysis each sample was kept at room temperature for 2 weeks.

The DSC traces of the so-treated samples are reported in Figure 7 and the results obtained in Table 3. In all cases, a glass transition and a melting endotherm are evident, with exception of PDGCE, whose DSC trace is characterized only by an endothermal baseline deviation associated with the glass transition phenomenon. In the case of PBCE, the endothermal shift of baseline related to the glass transition phenomenon is not well observable, due to the high crystallinity of this sample.

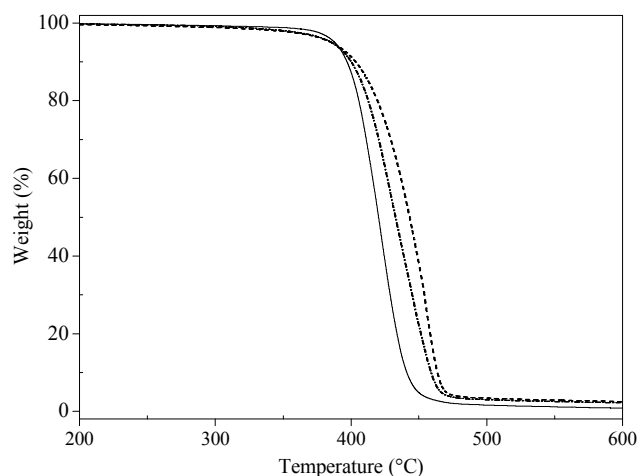


**Figure 6.** TGA curves under nitrogen atmosphere (10 °C/min): solid line: PBCE; dash: PDGCE; dash dot: P(BCE<sub>7</sub>DGCE<sub>7</sub>).

First of all, it has to be emphasized that the phase behavior of the two parent homopolymers is opposite: PBCE is semicrystalline, whereas PDGCE completely amorphous. As is well known, the crystallization capacity of a polymer is correlated to several factors, among these the symmetry of the polymeric chain. The introduction of ether-oxygen atoms along the PBCE polymer chains causes a significant reduction of the symmetry (the van der Waals radius of oxygen atom (1.4 Å) is indeed significantly lower than that of the neighbor  $-\text{CH}_2$  groups (2.0 Å)). As a consequence, the ability of crystallizing is completely undone in PDGCE.

As far as the P(BCE<sub>x</sub>DGCE<sub>y</sub>) copolymers are concerned, only one glass transition temperature is always clearly evident, independently of block length, suggesting the presence of a homogeneous amorphous state. The miscibility of the two components in the amorphous phase will be more accurately evaluated analyzing the thermal behavior of the samples after melt quenching (see below). Concerning the melting phenomenon, it can be noted that the endothermic process becomes broader and its peak shifts to lower temperature as the mixing time increases.

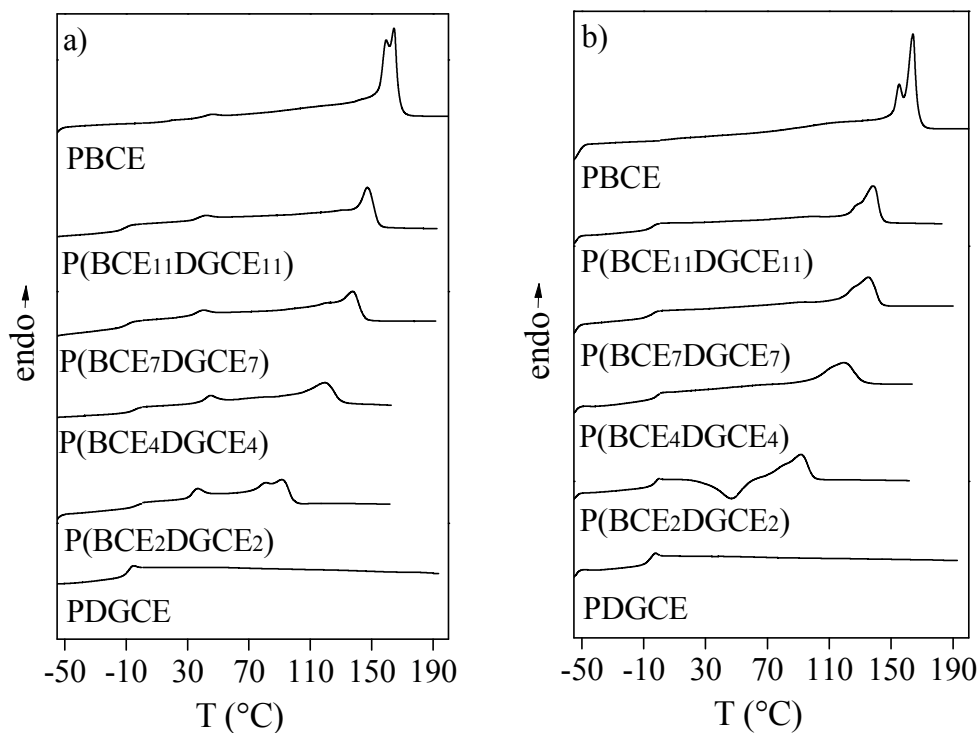


**Figure 7.** Calorimetric curves of PBCE, PDGCE and  $P(\text{BCE}_x\text{DGCE}_y)$  copolymers (heating rate: 20 deg/min): a) 1<sup>st</sup> scan; b) 2<sup>nd</sup> scan after melt quenching.

At lower temperature (about 40-50°C) a premelting endothermic peak, due to the fusion of poor perfection crystals, whose intensity increased as the block crystallizable length decreased, is also evident. Because PBCE crystallizes quite quickly, whereas PDGCE is completely amorphous under the experimental conditions adopted, the melting peaks observed in the copolymers can be attributed to the fusion of the crystalline phase of PBCE. Therefore, the decrement of the block length induces the formation of crystals with a low degree of perfection and a wide distribution of dimensions. As far as the heat of fusion is concerned, it has been found that it regularly decreased as the block length is decreased, indicating that PBCE crystallizes in the copolymers to a minor extent as in the pure state. Moreover, in the case of random copolymer ( $P(\text{BCE}_2\text{DGCE}_2)$ ), multiple melting endotherms are evident (in this case the highest peak temperature was taken as  $T_m$ ). Generally

speaking, the possible origin of the multiple melting peaks may be listed as follow: (a) presence of more than one crystal structure and (b) melt-recrystallization process occurring during the DSC scan. As previously reported,<sup>24</sup> the multiple melting endotherm phenomenon observed in PBCE has been ascribed to a reorganization process taking place during the DSC scan, due to a mechanism based on melting and recrystallization of less perfect crystallites into thicker crystals, followed by a final melting process at higher temperature. Therefore, the multiple melting peaks present in the DSC traces of the copolymer can be hypothesized to have the same origin.

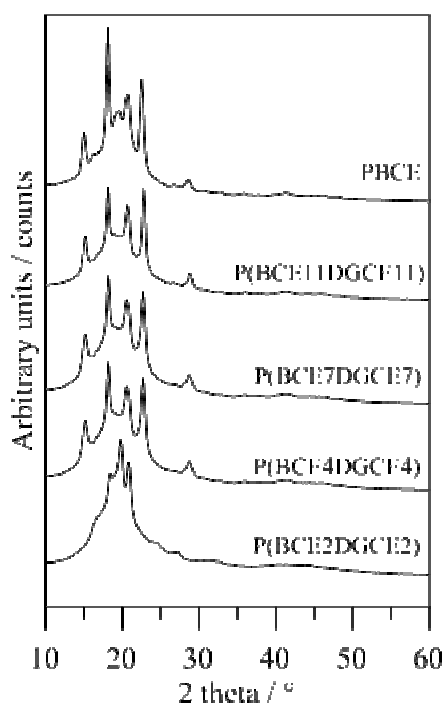


**Figure 8.** XRD patterns of PBCE and P(BCE<sub>x</sub>DGCE<sub>y</sub>) copolymers.

In order to more deeply investigate the nature of the crystalline phase in the polymers under investigation, X-ray analysis was performed. The X-ray diffraction profiles for PBCE and P(BCE<sub>x</sub>DGCE<sub>y</sub>) copolymers are reported in Figure 8: first of all, all the XRD patterns exhibit a well-defined and intense set of crystalline diffraction peaks, except P(BCE<sub>2</sub>DGCE<sub>2</sub>) random copolymer. In particular, the patterns of block copolymers show identical intense reflections at  $2\theta$

values of 15.2°, 18.1°, 20.7°, 22.8° (2 $\theta$ ) and a weaker one at 28.8°, with some small variations of the d-spacings not correlated to the block length. A strong similarity between the pattern of PBCE homopolymer and those of block P(BCE<sub>x</sub>DGCE<sub>y</sub>) copolymers is clear in Figure 8, even though the XRD spectrum of the homopolymer is characterized by other further reflections at 16.2°, 19.2° e 19.6°, not present in the copolymer spectra.

The random copolymer XRD spectrum is on the contrary significantly different, being characterized by a weak and broad reflection at 16.5° and by other ones at 18.5°, 19.8°, 20.8°. This result suggests the presence of a different crystal phase in this sample. Moreover, it can be hypothesized that the reflections at 16.2°, 19.2° e 19.6° present in the PBCE XRD spectrum are due to a further crystalline phase which has been observed in the random copolymer too.

Therefore, it can be concluded that in the case of block copolymers the presence of PDGCE units does not alter the kind of pattern and that the crystalline fraction is ordered in the same manner, i.e. the phase is PBCE, independently of the reaction time.

The crystallinity indexes for these copolymers are reported in Table 3, together with that of PBCE: the crystallinity index roughly decrease as the reaction time increases, i.e. the block length decreases, in agreement with the calorimetric results. No X<sub>C</sub> value is reported for the random copolymer, being this sample characterized by a different crystal phase.

As mentioned above, further considerations on miscibility can be done on the samples quenched from the melt. The corresponding DSC traces are shown in Figure 7b: as it can be seen, the calorimetric traces of PBCE and all block copolymers are characterized by a glass transition followed by a conspicuous melting endotherm. The DSC curve of random copolymer shows a glass transition followed by an exothermal 'cold crystallization' peak and a melting endotherm at a higher temperature. The enthalpy of crystallization compares well with the corresponding heat of fusion, indicating that this polymer is completely amorphous. As regards the calorimetric curve of pure

PDGCE, only an intense endothermal baseline deviation associated with the glass transition is observed.

Regarding the glass transition phenomenon, first of all, as it can be noted from Table 3, the introduction along the PBCE backbone of the ether-oxygen atoms causes a significant decrement of  $T_g$ . Anyway, such decrement cannot be explained on the basis of the different phase behaviour of PBCE (semicrystalline) in respect to PDGCE (amorphous). On the contrary, the high decrement of  $T_g$  has to be ascribed to differences in chemical structure: in particular, this trend can be correlated to the higher flexibility induced in the polymer chain by ether-oxygen atoms. As regards the copolymers, in all cases only one glass transition intermediate between those of pure parent homopolymers is evident, analogously to the first scan, confirming the complete miscibility in the amorphous phase. Looking into more detail, one can see that  $T_g$  value slightly increased as the block length decreased, indicating that the flexibility effect lessens with decreasing the block length.

To evaluate if the DGCE sequences affect the crystallizing capability of PBCE, non-isothermal experiments were carried out, subjecting the samples to the thermal treatment described in the Experimental Section. It is worth remembering that the half-time of primary crystallization in isothermal experiments correlates with the temperature corresponding to the maximum of the crystallization peak in non-isothermal experiments ( $T_{cc}$ ),<sup>32</sup> being this latter more easily obtainable. The exothermic crystallization peaks of the samples under investigation are reported in Figure 9: as it can be seen, the temperature corresponding to the maximum of the exothermal crystallization peak regularly decreases as the mixing time is increased, indicating that the crystallization process becomes more and more difficult as the PBCE blocks become progressively shorter and the copolymer tends toward a random distribution of the sequences.

This trend is due to the effect of the PDGCE sequences, which limits the transport of the PBCE chains on the crystal surface and act as a defect during chain folding. Therefore, in block copolymers, a decrement of the crystallization rate with a reduction of the block length is evident.

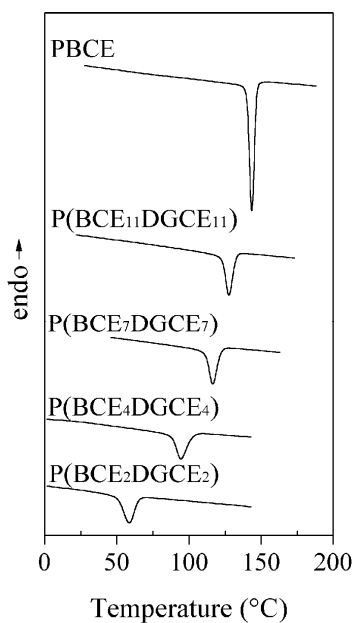


**Figure 9.** DSC crystallization exotherms of PBCE and P(BCE<sub>x</sub>DGCE<sub>y</sub>) copolymers cooled from the melt at 5°C/min.

### 3.3 Mechanical characterization

Tensile mechanical properties of PBCE, and P(BCE<sub>x</sub>DGCE<sub>y</sub>) copolymers are reported in Table 4, where elastic modulus,  $E$ , stress at break,  $\sigma_b$  and deformation at break,  $\varepsilon_b$  are listed.

**Table 4.** Mechanical characterization data PBCE, PDGCE and P(BCE<sub>x</sub>DGCE<sub>y</sub>) copolymers.

Polymer	$E$ (MPa)	$\sigma_b$ (MPa)	$\varepsilon_b$ (%)
PBCE	459 ± 11	33 ± 1	31 ± 11
P(BCE <sub>11</sub> DGCE <sub>11</sub> )	75 ± 14	7 ± 1	45 ± 10
P(BCE <sub>7</sub> DGCE <sub>7</sub> )	80 ± 7	9 ± 1	103 ± 26
P(BCE <sub>4</sub> DGCE <sub>4</sub> )	100 ± 7	10 ± 2	240 ± 66
P(BCE <sub>2</sub> DGCE <sub>2</sub> )	121 ± 5	15 ± 2	785 ± 74

PBCE homopolymer displayed the highest elastic modulus and it was the stiffest material among the synthesized polymers, with a relatively low deformation at break (31%). As concerns

copolymers, the elastic modulus and elongation to break regularly increase as the block length is decreased (see Figure 10).

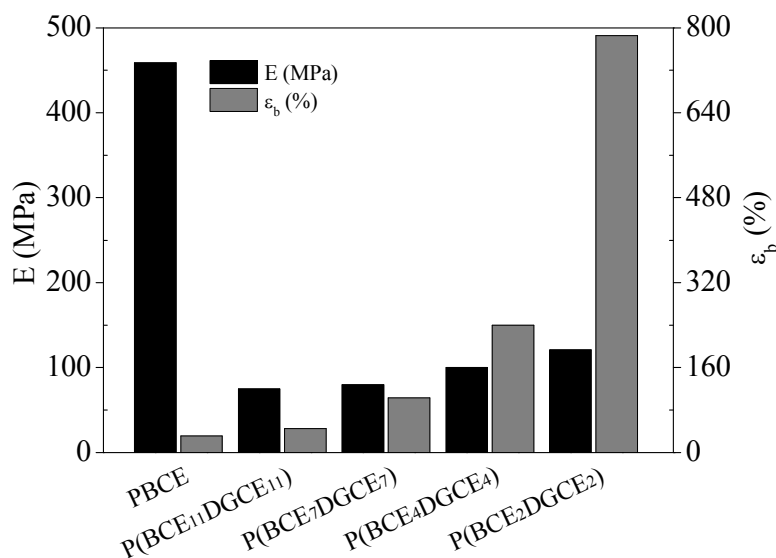


**Figure 10.** Elastic modulus ( $E$ ) and deformation to break ( $\epsilon_b$ ) of PBCE and P(BCE<sub>x</sub>DGCE<sub>y</sub>) copolymers.

Moreover, it is worth emphasizing that the random copolymer is characterized by an elastomeric behavior, with an extremely high deformation at break that reaches a value of about 800%. Overall, mechanical characterization demonstrated that the introduction of DGCE units into PBCE chains resulted in a significant change in the copolymer mechanical properties. However, mechanical behavior cannot be explained exclusively on the basis of BCE and DGCE block length. To gain further understanding of the results, mechanical properties were analyzed with the aid of the above reported thermal and structural characterization. All the investigated polymers displayed a mobile soft amorphous phase ( $T_g < RT$ ) and a rigid hard crystal phase. In particular, the observed trend can be explained as due to the following two effects: i) amount of crystal phase present in the material; ii) flexibility of the oxygen-containing sequence related to its length. Despite the decrease in the amount of crystal phase,  $E$  increases with the decreasing of block length. This effect this can be explained as due to the prevalent effect of a reduced flexibility of polymer chain. As a matter of

fact, the short ether-oxygen containing sequences are not anymore able to flexibilize at a significant degree the macromolecular chain.

### 3.4 Hydrolytic degradation studies

As previously reported,<sup>26</sup> PBCE homopolymer undergoes a very slow hydrolytic degradation under physiological conditions (37 °C and pH = 7.4).

In the present work, hydrolytic degradation experiments were performed under physiological conditions on the new P(BCE<sub>x</sub>DGCE<sub>y</sub>) copolymers in order to evaluate the effect of the introduction of hydrophilic DGCE units in the PBCE macromolecular chains and to investigate the effect of the unit block length on hydrolysis rate.

Weight losses are reported in Figure 11a as a function of time: as it can be seen, they are strongly affected by block length. In particular, the weight loss was higher with increasing block length. After about 180 days of degradation the residual weight was around 87% for P(BCE<sub>11</sub>DGCE<sub>11</sub>), 91% for P(BCE<sub>7</sub>DGCE<sub>7</sub>), 93% for P(BCE<sub>4</sub>DGCE<sub>4</sub>) and 98% P(BCE<sub>2</sub>DGCE<sub>2</sub>), while as expected, PBCE did not display a significant weight loss.

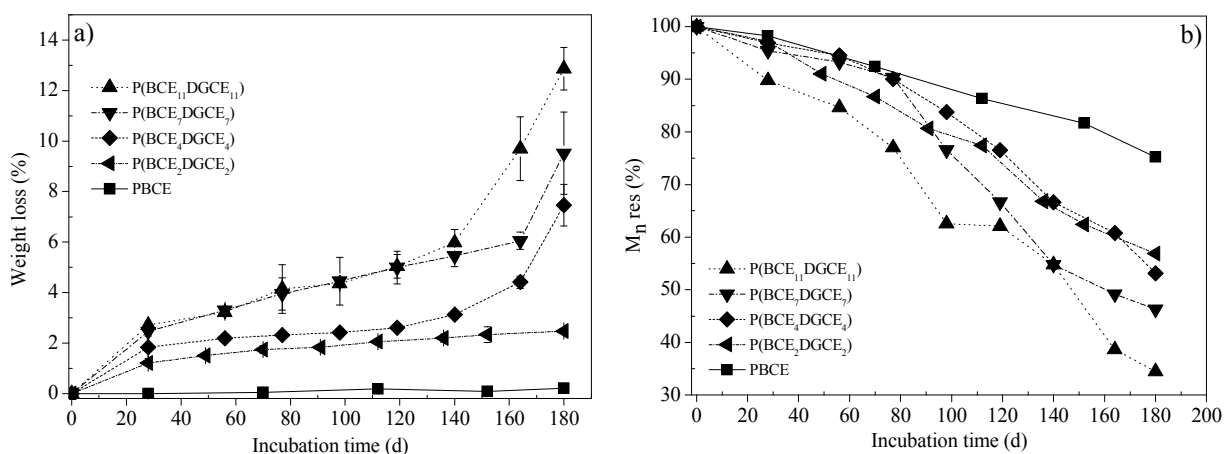


**Figure 11.** Weight loss (%) a), residual number molecular weight ( $M_n$  res%) b), as a function of incubation time.

It is worth mentioning that weight loss occurs when the hydrolysis of the ester bonds leads to the formation of water-soluble oligomers. Therefore, data in Figure 11a demonstrated that, at the same degradation time, the hydrolysis of copolymers with longer blocks generated oligomers that were either shorter or more soluble than those generated from copolymers with shorter blocks. The percentage of residual number average molecular weight ( $M_n$ ,res%) is reported in Figure 11b as a function of time. All the samples, including PBCE, underwent a decrease of  $M_n$  with time: it is in fact well known<sup>33</sup> that in the first stages of hydrolytic degradation a substantial decrease in the molecular weight occurs, even if weight losses are still negligible. PBCE was less affected by this phenomenon in the time scale explored, due to its high crystallinity degree, high crystal perfection and hydrophobicity (Table 3), while in the case of copolymers, the change of molecular weight was more evident and it seemed to be affected by block length. In particular, shorter blocks led to a minor decrease in  $M_n$ .

In order to gain a better understanding of the hydrolysis mechanism of the copolymers, <sup>1</sup>H-NMR measurements were performed on degraded retrieved samples.

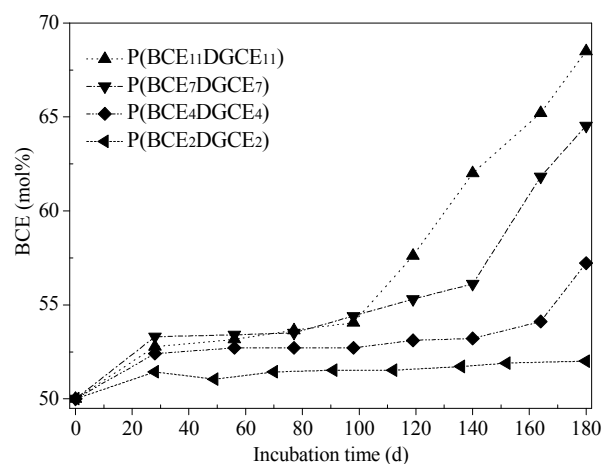


**Figure 12.** BCE mol% content in P(BCE<sub>x</sub>DGCE<sub>y</sub>) copolymers as a function of incubation time.

Figure 12 reports the content of BCE units in mol% as a function of degradation time. An evident increase of BCE content was observed during degradation. This was more consistent for samples

with longer blocks. In particular, after about 180 days of water exposure, the amount of BCE units increased from the initial 50 mol% of the non-degraded samples up to 56%, 63%, and 68 % for P(BCE<sub>4</sub>DGCE<sub>4</sub>), P(BCE<sub>7</sub>DGCE<sub>7</sub>) and P(BCE<sub>11</sub>DGCE<sub>11</sub>), respectively. The chemical composition of P(BCE<sub>2</sub>DGCE<sub>2</sub>) remained constant.

Hydrolytic degradation of P(BCE<sub>x</sub>DGCE<sub>y</sub>) copolymers can be interpreted on the basis of BCE and DGCE block length. The changes of chemical composition (Figure 12) together with the weight losses (Figure 11a) showed that a higher increase of BCE unit content in the course of the degradation corresponded to a higher weight loss. Therefore, the weight loss was mainly due to the solubilisation of chain fragments having a high content of DGCE units. Consequently, ester cleavage preferentially occurred on chain segments containing long DGCE sequences, which, due to their hydrophilic nature, were easily solubilised in water. The molecular weight decrease (Figure 11b) was higher for copolymers with longer blocks while copolymers with shorter blocks underwent a lower molecular weight loss. Similarly to poly(lactide-co-glycolide) copolymers, where G–G ester bonds are more easily hydrolyzed than G–L ones,<sup>34</sup> it is possible to assume that DGCE–DGCE ester bonds were preferentially cleaved compared to DGCE–BCE bonds, the latter being at higher concentration in polymers with shorter blocks.

### 3.5 Biocompatibility and gene expression assays

The PrestoBlue<sup>®</sup> fluorescence assay was used to estimate the potential indirect cytotoxicity of neat PBCE and P(BCE<sub>x</sub>DGCE<sub>y</sub>) co-polymers on H9c2 cells.

As shown in Fig. 13a, data indicate the absence of potentially cytotoxic products released from any of the polymers into the culture medium. In fact, the fluorescence output of the assay, expressed as arbitrary units (a. u.) was comparable for samples grown for 48 h in neat PBCE, P(BCE<sub>2</sub>DGCE<sub>2</sub>), P(BCE<sub>4</sub>DGCE<sub>4</sub>), P(BCE<sub>7</sub>DGCE<sub>7</sub>) and P(BCE<sub>11</sub>DGCE<sub>11</sub>) extraction medium (40810 ± 3595, 40720 ± 3974, 39020 ± 4914, 42240 ± 3137, 43170 ± 1830 and 37130 ± 2970 respectively) and equivalent to the value obtained for the standard DMEM control (41560 ± 3598). On the other hand, when

exposed to 1 mM H<sub>2</sub>O<sub>2</sub> for 120 min, as a positive cytotoxicity control, all the cells were killed (data not shown).

PrestoBlue<sup>®</sup> fluorescence assay was also used to evaluate cell adhesion and proliferation: quantification was performed by fluorescence measurements (expressed in arbitrary units) on samples measured at day 1, 7 and 14.

The results reported in Fig. 13b show that, after 24 h from cell seeding, all films host about the same number of H9c2 cells [PBCE: 5161 ± 312.6 a. u.; P(BCE<sub>2</sub>DGCE<sub>2</sub>): 4591 ± 180.5 a. u.; P(BCE<sub>4</sub>DGCE<sub>4</sub>): 4663 ± 436 a. u.; P(BCE<sub>7</sub>DGCE<sub>7</sub>): 5126 ± 546.1 a. u.; P(BCE<sub>11</sub>DGCE<sub>11</sub>): 4574 ± 145.1 a. u.] [PS= 10260 ± 386.1 = gg 1; 57030 ± 1425 = gg 7; 99320 ± 741.6 = gg 14].

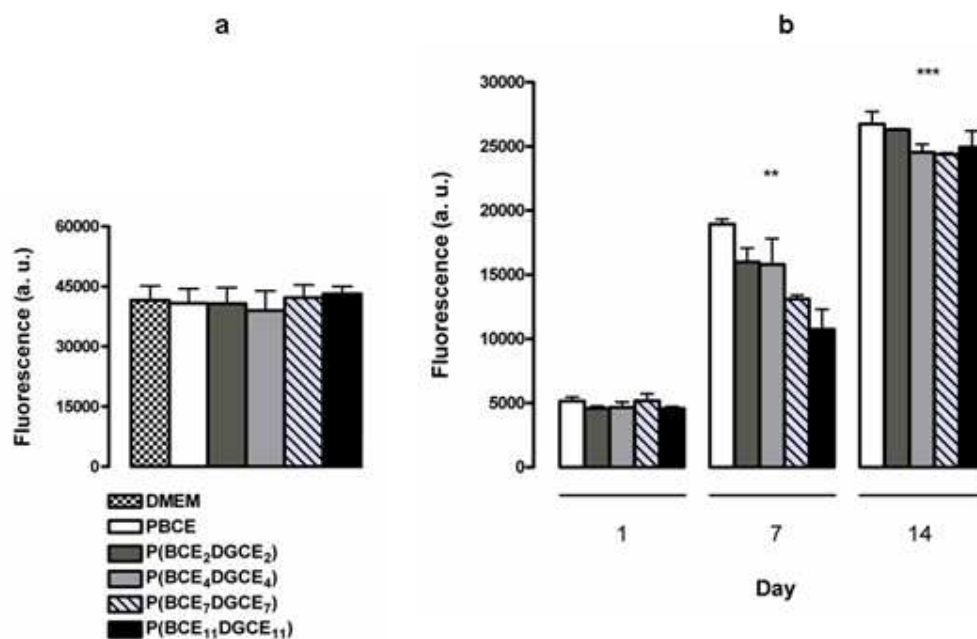


**Figure 13.** a) Evaluation of indirect cytotoxicity; b) Proliferation assay. At day 7, \*\* = significantly different ( $P < 0.01$ ) versus day 1. At day 14, \*\*\* = significantly different ( $P < 0.001$ ) versus day 1 and 7 ( $P < 0.05$ ).

At day 7 [PBCE: 18950 ± 384.1 a. u.; P(BCE<sub>2</sub>DGCE<sub>2</sub>): 16000 ± 1078 a. u.; P(BCE<sub>4</sub>DGCE<sub>4</sub>): 16790 ± 3037 a. u.; P(BCE<sub>7</sub>DGCE<sub>7</sub>): 13110 ± 288.3 a. u.; P(BCE<sub>11</sub>DGCE<sub>11</sub>): 10750 ± 1570 a. u.] and at the

end of experiments (day 14) [ $26750 \pm 962.3$  a. u.,  $26310 \pm 60.25$  a. u.,  $24930 \pm 1275$  a. u. ,  $24540 \pm 620.8$  a. u. and  $24390 \pm 112.8$  a. u. for neat PBCE, P(BCE<sub>2</sub>DGCE<sub>2</sub>), P(BCE<sub>4</sub>DGCE<sub>4</sub>), P(BCE<sub>7</sub>DGCE<sub>7</sub>) and P(BCE<sub>11</sub>DGCE<sub>11</sub>) respectively] the trend resulted almost unchanged. All samples equally sustained cell proliferation.

The production and the accumulation of the typical skeletal muscle marker of terminal differentiation - total sarcomeric myosin heavy chain (MHC) – has been analysed in several studies to attest the effect of mechanical conditioning and/or physicochemical features of polymeric substrates on the development of skeletal muscle engineered constructs.<sup>35-36</sup>

In our experimental conditions, real time PCR data on myosin heavy chain expression, marker of a muscle phenotype appeared up to fourfold increased versus PBCE, P(BCE<sub>2</sub>DGCE<sub>2</sub>) and P(BCE<sub>11</sub>DGCE<sub>11</sub>) when cells were cultured for 14 days adhering on P(BCE<sub>4</sub>DGCE<sub>4</sub>) and P(BCE<sub>7</sub>DGCE<sub>7</sub>) (Figure 14).

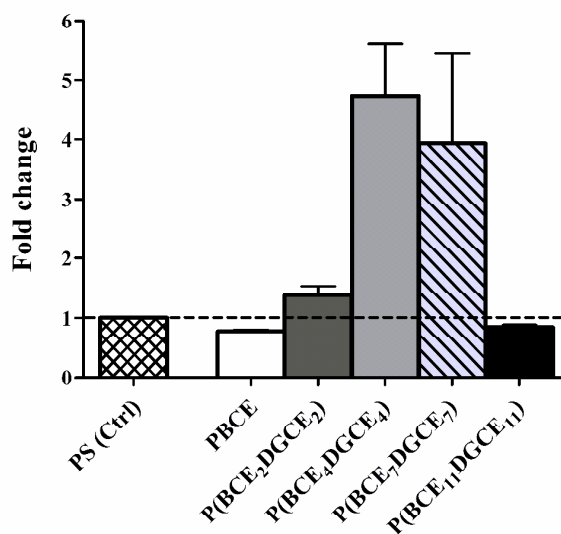


**Figure 14.** Real time PCR data on myosin heavy chain expression.

#### 4. CONCLUSIONS

The synthesis of new P(BCE<sub>x</sub>DGCE<sub>y</sub>) multiblock copolyesters demonstrated the potentialities of reactive blending as a simple, economic, and versatile synthetic route that ensures accurate tailoring of block length by controlling the reaction time. For this series of copolyesters possessing the same chemical composition, thermal and mechanical properties, surface wettability, and hydrolysis rate have been tailored by simply varying block length, i.e. mixing time.

In terms of mechanical properties, we were able to synthesize polyesters whose stiffness and deformability can be tailored by controlling the crystallinity degree and the length of DGCE flexible block. Block length has a remarkable effect in defining both surface hydrophilicity and hydrolysis rate. Indeed, *in vitro* degradation experiments performed over a period of 180 days showed that polymer mass loss can be tuned from 0 to 13% by simply increasing block length. Therefore, materials with different degradation rates are available: P(BCE<sub>11</sub>DGCE<sub>11</sub>) and P(BCE<sub>7</sub>DGCE<sub>7</sub>) are particularly promising for short-term applications, P(BCE<sub>2</sub>DGCE<sub>2</sub>) can be used for long-term applications whereas the remaining copolymer has intermediate degradation times.

Moreover, biocompatibility assays performed in accordance with the ISO10993-5 international standard for biological evaluation of medical devices showed the absence of potentially cytotoxic products released into the culture medium by the investigated samples, and demonstrated that our substrates support a physical environment where cells can adhere and proliferate. Myosin heavy chain expression, a marker of a muscle phenotype appeared significantly enhanced in cells seeded onboard of copolymers with specific combinations of elasticity/deformability, namely P(BCE<sub>4</sub>DGCE<sub>4</sub>) and P(BCE<sub>7</sub>DGCE<sub>7</sub>). This result confirms that the tuning of polymer physicochemical features play an important role when the activation of a specific gene expression program is a desirable attribute for a biomaterial. Prospectively, evaluation of processability through scaffold-manufacturing techniques (see e.g. Focarete et al.<sup>37</sup>) and/or testing in dynamic cell

culture settings (see e.g. Govoni et al.<sup>38-39</sup>) will be important further steps in order to confirm the potential value of these new copolyesters in soft tissue engineering.

## References

- 1) L.A. Smith, X. Liu, P.X. Ma, *Soft Matter*, 2008, **4**, 2144-2149.
- 2) J.W. Nichol, A. Khademhosseini, *Soft Matter*, 2009, **5**, 1312-1319.
- 3) R.H. Harrison, J.P. St-Pierre, M.M. Stevens, *Tissue Eng Pt B-Rev*, 2014, **20**, 1-16.
- 4) J.K. Oh, *Soft Matter*, 2011, **7**, 5096-5108.
- 5) D.G. Barrett, M.N. Yousaf, *Soft Matter*, 2010, **6**, 5026-5036.
- 6) T. Garg, A.K. Goyal, *Expert Opin Drug Del*, 2014, DOI: 10.1517/17425247.2014.891014.
- 7) P. Lei, H. You, and S. T. Andreadis in *Organ Regeneration: Methods and Protocols*, ed. J. Basu and J. W. Ludlow, Springer, New York, 2013, vol. 1001, ch. 22, pp. 267–278.
- 8) N.J. Panetta, D. M. Gupta, M. T. Longaker, *Curr Stem Cell Res Ther*, 2010, **5**, 122–128.
- 9) D. Eglin, D. Mortisen, M. Alini, *Soft Matter*, 2009, **5**, 938-947.
- 10) R.T. Tran, P. Thevenot, D. Gyawali, J.C. Chiao, L. Tang, J. Yang, *Soft Matter*, 2010, **6**, 2449-2461.
- 11) Z. Ma, Y. Hong, D.M. Nelson, J.E. Pichamuthu, C.E. Leeson, W.R. Wagner, *Biomacromolecules*, 2011, **12**, 3265-3274.
- 12) A. Jaeger, D. Gromadzki, E. Jaeger, F.C. Giacomelli, A. Kozłowska, L. Kobera, J. Brus, B. Rihova, M. El Fray, K. Ulbrich, P. Stepanek, *Soft Matter*, 2012, **8**, 4343-4354.
- 13) C. Liu, Z. Zhang, K.L. Liu, X. Ni, J. Li, *Soft Matter*, 2013, **9**, 787-794.
- 14) M.J. Pereira, B. Ouyang, C.A. Sundback, N. Lang, I. Friehs, S. Mureli, I. Pomerantseva, J. McFadden, M.C. Mochel, O. Mwizerwa, P. Del Nido, D. Sarkar, P.T. Masiakos, R. Langer, L.S. Ferreira, J.M. Karp, *Adv Mater*, 2013, **25**, 1209-1215.
- 15) D.K. Dempsey, J.L. Robinson, A.V. Iyer, J.P. Parakka, R.S. Bezwada, E.M. Cosgriff-Hernandez, *J Biomater Sci-Polym E*, 2014, **25**, 535-554.
- 16) M. Gigli, N. Lotti, M. Gazzano, L. Finelli, A. Munari, *J Appl Polym Sci*, 2012, **126**, 686–696.

- 17) M. Soccio, N. Lotti, M. Gigli, L. Finelli, M. Gazzano, A. Munari, *Polym Int*, 2012, **61**, 1163–1169.
- 18) M. Gigli, N. Lotti, M. Gazzano, L. Finelli, A. Munari, *Polym Eng Sci*, 2013, **53**, 491-501.
- 19) C. Gualandi, M. Soccio, E. Saino, M. L. Focarete, N. Lotti, A. Munari, L. Moroni, L. Visai, *Soft Matter*, 2012, **8**, 5466-5476.
- 20) M. Gigli, A. Negroni, M. Soccio, G. Zanaroli, N. Lotti, F. Fava and A. Munari, *Green Chem*, 2012, **14**, 2885-2893.
- 21) M. Gigli, N. Lotti, M. Gazzano, L. Finelli, Andrea Munari, *React Funct Polym*, 2012, **72**, 303–310.
- 22) M. Gigli, A. Negroni, G. Zanaroli, N. Lotti, F. Fava and A. Munari, *React Funct Polym*, 2013, **73**, 764-771.
- 23) M. Gigli, A. Negroni, M. Soccio, G. Zanaroli, N. Lotti, F. Fava and A. Munari, *Polym Degrad Stab*, 2013, **98**, 934-942.
- 24) M. Gigli, N. Lotti, M. Gazzano, V. Siracusa, L. Finelli, A. Munari, M. Dalla Rosa, *Ind Eng Chem Res*, 2013, **52**, 12876–12886.
- 25) C. Berti, A. Celli, P. Marchese, E. Marianucci, G. Barbiroli and F. Di Credico, *Macromol Chem and Phys*, 2008, **209**, 1333–1344.
- 26) M. Gigli, N. Lotti, M. Vercellino, L. Visai, A. Munari, *Mater Sci Eng C*, 2014, **34**, 86-97.
- 27) F. Bonavita, C. Stefanelli, E. Giordano, M. Columbaro, A. Facchini, F. Bonafè, C.M. Caldarera, C. Guarnieri, *FEBS Lett*, 2003, **536**, 85-91.
- 28) M. Govoni, F. Bonavita, L.M. Shantz, C. Guarnieri, E. Giordano, *Amino Acids*, 2010, **38**, 541-547.
- 29) M. Soccio, N. Lotti, M. Gazzano, M. Govoni, E. Giordano, A. Munari, *React Funct Polym*, 2012, **72**, 856-867.

- 30) C. Gualandi, M. Govoni, L. Foroni, S. Valente, M. Bianchi, E. Giordano, G. Pasquinelli, F. Biscarini, M.L. Focarete, *Eur Polym J*, 2012, **48**, 2008-2018.
- 31) A. Pasini, F. Bonafè, M. Govoni, C. Guarnieri, P.G. Morselli, H.S. Sharma, C.M. Calderera, C. Muscari, E. Giordano, *Cell Biochem Biophys*, 2013, **67**, 255-262.
- 32) R. Legras, J.M. Dekoninck, A. Vanzieleghem, J.P. Mercier, E. Nield, *Polymer*, 1986, **27**, 109-117.
- 33) M. Mochizuki, M. Hiram, *Polym Adv Technol*, 1997, **8**, 203-209.
- 34) J. Li, R. M. Styshich, T. Y. Meyer, *J Am Chem Soc*, 2011, **133**, 6910-6913.
- 35) S.A. Riboldi, M. Sampaolesi, P. Neuenschwander, G. Cossu, S. Mantero, *Biomaterials*, 2005, **26**, 4606-4615.
- 36) G. Candiani, S.A. Riboldi, N. Sadr, S. Lorenzoni, P. Neuenschwander, F.M. Montevecchi, S. Mantero, *J Appl Biomater Biom*, 2010, **8**, 68-75.
- 37) M.L. Focarete, C. Gualandi, M. Scandola, M. Govoni, E. Giordano, L. Foroni, S. Valente, G. Pasquinelli, W. Gao, R.A. Gross, *J Biomat Sci-Polym E*, 2010, **21**, 1283–1296.
- 38) M. Govoni, F. Lotti, L. Biagiotti, M. Lannocca, G. Pasquinelli, S. Valente, C. Muscari, F. Bonafè, C.M. Calderera, G. Guarnieri, S. Cavalcanti, E. Giordano, *J Tissue Eng Regen Med*, 2012, DOI: 10.1002/term.1578
- 39) M. Govoni, C. Muscari, G. Guarnieri, E. Giordano, *Biomed Res Int*, 2013, DOI: 10.1155/2013/918640.